



Super achromatic wide-angle quarter-wave plates using multi-twist retarders

LINGSHAN LI AND MICHAEL J. ESCUTI*

Department of Electrical and Computer Engineering, North Carolina State University, Raleigh, NC 27695,
USA

*mjescuti@ncsu.edu

Abstract: The achromaticity and wide-angle property of quarter-wave plates (QWPs) are crucial for the color uniformity and image resolution of the future displays such as virtual reality (VR) pancake lens and augmented reality (AR) waveguide/focusing systems. However, most reported achromatic wide-angle QWPs designs composed by stacks of different birefringent plates are too complicated with limited achromaticity and wide-angle performance. The multi-twist retarders (MTR) QWPs presented in previous work already showed its potential to achieve high achromaticity in RGB using one monolithic film in normal incidence, but the incompetent polarization control in blue-violet limits its application in LED-based polarization-sensitive AR/VR headsets. In this work, we theoretically investigate a new type of MTR QWPs achieving super achromaticity from violet to red with average ellipticity 43° and simultaneously maintaining wide-viewing angle up to $\pm 45^\circ$, which enables a precise polarization control within the field-of-view (FOV) of current AV/VR headset. The new proposed MTR QWP is also reported to obtain average reflection luminance leakage $0.15\sim\%$ and maximum leakage $0.23\sim\%$, making it a promising element to reduce polarization leakage and enhance image resolution in the next-generation displays.

© 2021 Optical Society of America under the terms of the [OSA Open Access Publishing Agreement](#)

1. Introduction

In the next-generation displays, as the light can be manipulated based on wavelength or polarization, the role of quarterwave plates (QWPs) becomes more versatile. In stereoscopic 3D displays, the achromatic QWPs to generate orthogonal circular polarization to remove the head-tilt effect [1,2]. In virtual reality (VR) pancake lens system, the achromatic QWPs is crucial to form the three-fold path to minimize the Petzval field curvature [3–5]. In augmented reality (AR) applications, as the transmissive/reflective Bragg polarization gratings become popular candidates for input/output coupler [6,7] and geometric phase (GP) lens is used to form image based on orthogonal circular polarization [8–10], the achromatic QWPs become an indispensable elements for these applications.

In the above scenarios, the image resolution is highly influenced by the achromaticity and viewing angle of the QWPs. As in current VR/AR applications, LED displays remains as the most popular option of light source [11], for it will not generate speckle noise [12] or interference pattern on the output image, which can be a major issue of laser diode (LD) with high temporal coherence [13]. However, the unignorable bandwidth of blue LED (around 20 nm) suggests that a competent QWPs in these systems should exhibit super achromaticity from violet to red. Considering the photometric response of blue is relatively low, any polarization leakage of blue caused by the incompetence of the QWPs can be detrimental to the color uniformity of the rendering image. The polarization leakage of blue is even more critical considering the off-axis blue rays often suffer significant back-coupling loss within the input coupler [14] and the FOV is often compromised. Therefore, maintaining super achromaticity from violet to red and wide-viewing angle is equivalently important for the AR systems to maintain color uniformity.

Considering the state of art of largest FOV is around $\pm 50^\circ$ for the VR systems [15] and $\pm 45^\circ$ for the AR systems [16], the largest wide-viewing angle of QWPs should be also within this range.

However, high achromaticity and wide-angle property is often a trade-off when using conventional birefringent stack plates. The achromatic QWPs composed by several layers of birefringent plates, either DP design [17] or Pancharatnam QHQ design [18], is based on the optimization of on-axis retardation, and unavoidably suffers severe retardation deviation in oblique incidence.

To achieve wide-angle performance of the achromatic QWPs, several other strategies have been reported. achromatic QWPs composed by uniaxial plates [19] and phase compensation film was reported to achieve certain wide-angle performance but suffered from limited acceptance angle and low contrast ratio (CR). Biaxial QWPs [1,20–22] followed the rule of minimizing out-of-plane retardation (R_{th}) are also reported to slightly enlarge the acceptance angle. More complicated design with the combination of optimized waveplates, and negative c -plate, a -plate and biaxial plates which adopted the phase compensation of method to satisfy the broadband circular polarizer condition ($2\phi_{\lambda_4} - 4\phi_{\lambda_2} = \pm\pi/2$) on wide-angle range, significantly improved the wide-angle performance, but at the cost of huge complexity [23–25]. Although recently some simplified version was reported [26], all these designs do not report high achromaticity in violet range. Besides, these reported designs often require various categories of birefringent plates, suffer unavoidable reflection loss and cannot meet the compactness requirement of the wearable headset. What's more, in the VR pancake lens system where the 50% mirror and QWPs is used [3], the reflection leakage is also important for it can significantly degrade the output intensity. Therefore, an ideal QWP for the AR/VR/MR system should have the following characteristics: high-achromatic, and wide-angle, compact, and low reflection leakage.

In this work, two new designs of monolithic QWPs are proposed based on the optimization of Mueller matrix cost function and validated using extended Jones matrix. The achromaticity and wide-angle performance are investigated through a comparison including one classic QWPs design, one type of previous MTR QWP and two other new proposed QWPs. Within these four designs, we find that one new proposed MTR QWP to have best achromaticity and wide-viewing angles and meet the requirement of polarization control and FOV of the current AR/VR systems. Compared to previous work [27], there are three central advances of this work. First, the achromaticity is extended to violet, compared to only RGB in previous work. Second, the wide-viewing property of the MTR QWPs is theoretically proven to match the FOV requirement of the AR/VR applications. Third, the luminosity leakage of MTR QWPs is studied the first time, which shows the new proposed MTR QWPs has a much lower leakage than the current state of art.

2. Background

2.1. Multi-twist retarders concept

Liquid crystal multi-twist retarders(MTRs) (Fig. 1) is an optical component that can offer retardation control for broadband by aligning subsequent LC layers to previous layers and forming a monolithic film [27,28]. The amplitude and phase of the input light is modified when transmitting through MTRs. Such mechanism can be described by the MTRs Mueller matrix \mathbf{M} . If we have a MTR with m layers, mathematically the whole MTRs Mueller matrix \mathbf{M} is the product of the Mueller matrix of each homogeneous LC unit from bottom to top as follows:

$$\mathbf{M} = \mathbf{M}_m \dots \mathbf{M}_2 \mathbf{M}_1. \quad (1)$$

Here, the matrix of each MTR layer \mathbf{M}_m is a function of its twist Φ_m and thickness d_m plus the initial angle Φ_0 . The twist $\Phi_m = 0$ indicates a non-chiral homogeneous layer, and a chiral layer with an uniform twist rate is represented by a non-zero Φ_m . Counting m layers of MTR, there are $2m + 1$ parameters in total for the whole MTR Mueller matrix. The optimization of the MTR

structure is implemented and a global optimal solution is achieved based on the global fitting of these $2m + 1$ parameters of a customized cost function.

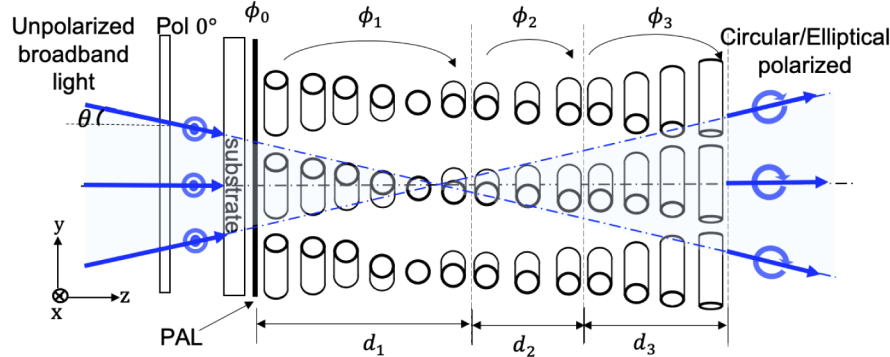


Fig. 1. Unpolarized broadband light become horizontal polarized light after incident onto horizontal polarizer Pol 0° , and transmits through MTR QWPs with design parameter ($\phi_0, \phi_1, d_1, \phi_2, d_2, \phi_3, d_3$), resulting in broadband circular/elliptical polarized light.

2.2. Extended Jones matrix method

To evaluate the quarter-wave achromatic performance of the MTR QWPs at oblique incidence, extended Jones matrix is an ideal method for analysis. Within this analysis, the MTR QWPs can be simulated as the combination of *a*-plate resembling the nonchiral layer, and twist-nematic (TN) liquid crystal cell resembling the self-aligning chiral twist layer.

In this analysis, several assumptions have been made. First, only reflection on the first surface of the QWP is considered, while the internal reflection within other sub-layers being ignored. Second, small birefringence is assumed as $|n_e - n_o| \ll n_o, n_e$. Under such condition, there is almost no reflection loss between the polarizer and the MTR QWP front surface.

As mentioned above, MTR structure can be composed by arbitrary sequence and number of nonchiral or chiral layers. For description convenience, we use m as the index of MTR layer, and l as the index of sublayer within a specific MTR layer. With the above assumptions, if the m th MTR layer is a chiral layer composed of l sublayers of birefringent *a*-plate (thickness d_l), it resembles the l -sublayer TN cell and can be described by an extended Jones matrix of \mathbf{J}_m as :

$$\mathbf{J}_m = \mathbf{P}_l \mathbf{D}_{(l-1),l} \mathbf{P}_{(l-1)} \mathbf{D}_{(l-2),(l-1)} \dots \mathbf{D}_{1,2} \mathbf{P}_1. \quad (2)$$

The dynamic matrix $\mathbf{D}_{l,(l-1)}$ is the cross-coupling from the local coordinate $(\mathbf{o}_{l-1}, \mathbf{e}_{l-1})$ of $(l-1)$ th sublayer, to the $(\mathbf{o}_l, \mathbf{e}_l)$ of l th sublayer. The propagation matrix \mathbf{P}_l represents the diagonal conventional Jones matrix of the l th birefringent plate with matrix element calculated as $\mathbf{P}_{l[1,1]} = \exp(i k_{ez} d_l)$ and $\mathbf{P}_{l[2,2]} = \exp(i k_{oz} d_l)$, with k_{ez} and k_{oz} is the \mathbf{z} -component wave vector k_z of \mathbf{o} wave and \mathbf{e} wave respectively. Therefore, the propagation matrix \mathbf{P}_l is both wavelength-dependent and incident-angle-dependent.

The extended Jones matrix \mathbf{J} of the whole MTR structure that transfers the input electric field vector of isotropic medium local coordinate (\mathbf{s}, \mathbf{p}) to another isotropic medium output local coordinate $(\mathbf{s}', \mathbf{p}')$ can be defined as:

$$\begin{bmatrix} A_{s'} \\ A_{p'} \end{bmatrix} = \mathbf{J} \begin{bmatrix} A_s \\ A_p \end{bmatrix} = \mathbf{D}_o \mathbf{J}_m \mathbf{D}_{[m,m-1]} \mathbf{J}_{m-1} \dots \mathbf{J}_2 \mathbf{D}_{[2,1]} \mathbf{J}_1 \mathbf{D}_i \begin{bmatrix} A_s \\ A_p \end{bmatrix}. \quad (3)$$

The dynamic input matrix \mathbf{D}_i and output matrix \mathbf{D}_o is the cross-coupling of electric field vector of (\mathbf{s}, \mathbf{p}) and $(\mathbf{s}', \mathbf{p}')$ to the local coordinate of the neighboring birefringent plate (\mathbf{o}, \mathbf{e}) ,

respectively. Similarly, the dynamic matrix $\mathbf{D}_{[m,m-1]}$ is the (\mathbf{o}, \mathbf{e}) cross-coupling between the last sublayer of the $(m-1)$ th MTR layer and the first sublayer of the m th MTR layer.

With the extended Jones matrix, one can also investigate influence of polarizer on wide-angle performance. The polarizer/analyzer can be simulated as ideal O-typed polarizer (complex index $\tilde{n}_{po} = n_{po} + ik_{po}$, $\tilde{n}_{pe} = n_{pe} + ik_{pe}$, real index $n_{po} = n_{pe}$, extinction ratio $k_{po} = 0$, $0 < k_{pe} \ll 1$), which adhered to the QWPs front/back surface. The polarizer index is set as $n_{po} \approx n_o$, with n_o as MTR QWP ordinary index. To summarize, given a specified wavelength and incident angle, the extended Jones matrix \mathbf{J} can be determined, and the output transmission and other polarization properties can be investigated. Therefore, the phase retardation Γ is a function of wavelength λ , incident angle (θ, ϕ) and MTR parameters as:

$$\Gamma = \sum_{m=1}^{\infty} f(\Delta n(\lambda), n_o(\lambda), n_e(\lambda, \theta, \phi), \phi_0, d_m, \phi_m). \quad (4)$$

3. Multi-twist retarders quarter-wave plates design

To achieve achromatic QWPs design, an optimization process is implemented by finding the global minimum of a designed merit function, which expressed as $2m+1$ parameters of m layers of MTR structure. The determination of merit function usually based on the polarization ellipse generated by QWPs. For QWPs that transform horizontal linear polarized state from $(S_i = (S_0, S_1, S_2, S_3)^T)$ to $(S'_i = (S'_0, S'_1, S'_2, S'_3)^T)$, ellipticity angle χ can be represented by the Stokes vector as:

$$\sin 2\chi = S'_3/S'_0. \quad (5)$$

A perfect QWPs should have maximum S'_3 approximating to 1, leading to

$$\tan \chi = 1. \quad (6)$$

In an optimization process, a merit function needs to be constructed to address the specific requirement. According to the design requirement stated above, the merit function should ensure the average output ellipticity $\bar{\chi}$ of four central wavelength obtained its optimal value 45° . There are numerous ways to construct merit function based on this requirement. One of the possible merit function can be as follows:

$$f = \overline{|1 - \tan[(1/2) \cdot \sin^{-1}(S_{t3}/S_{t0})]|}. \quad (7)$$

It should be noted that this merit function is varied by wavelength as $f = f(\lambda)$. For a certain wavelength λ_t that incident onto the MTR QWPs and the perfect quarter-wave retardation is achieved, the value S_{t3}/S_{t0} is 1, forcing the related merit function $f(\lambda_t) = 1$. Therefore, the optimization problem is a process of searching for design variables that can give the minimum merit functions in central wavelength. In our simulation, these central wavelength is specified as: $\lambda_c = 420$ nm, 457 nm, 533 nm, 636 nm.

Before starting the optimization process, we first identify the variables and the design parameters. The variables are the thickness d_m and twist angle ϕ_m of every MTR layer. The design parameters include the birefringence of QW 3TR-C, which is chosen as $\Delta n_C(\lambda) = 0.17 + 20647/\lambda^2$, while the birefringence of QW3TR-D is chosen as: $\Delta n_D(\lambda) = 0.19 + 15660/\lambda^2$.

To start the design process, we first employ the Mueller matrix of the MTR structures [27], a function of design variables $(d_1, d_2, \dots, d_m, \phi_1, \phi_2, \dots, \phi_m)$, to multiply the input Stokes vector, which set as either linear polarized or circular polarized light. The output Stokes vector can thus be calculated based on the random seed of variables. The matlab function *fminsearch* is used to find the global minimum of the merit function, and finally determine an optimal solution of design variables. Two 3TR-QWPs designs are achieved and listed in Table 1.

Table 1. Quarter Wave Plate (QWPs) Design

Design	$\phi_0(^{\circ})$	$\phi_1(^{\circ})$	$d_1(\mu m)$	$\phi_2(^{\circ})$	$d_2(\mu m)$	$\phi_3(^{\circ})$	$d_3(\mu m)$
3TR QW-C	16	0	0.74	60	0.25	0	0.31
3TR QW-D	0	12.9	1.08	47.4	0.88	251	1.07

4. Results

This section employs extended Jones matrix to simulate four types of QWPs for comparison. The first type of QWPs in comparison is the classic HQ design, first presented by Destrau and Prouteau [17] and widely in displays industries [20,21,29–31]. Other three include one MTR QWPs (3TR QW-A) in prior work [27], and two new designed MTR QWPs. The whole simulation is implemented in *Matlab* and the validation of several basic elements have been demonstrated in [Supplement 1](#) Section 1.

4.1. Normal incidence

A perfect QWP transfers the linear polarized light into circular polarized light, or vice versa. To compare the achromaticity and wide-angle property of quarter-wave performance of the design, several parameters have been investigated in normal incidence.

Two references are added into comparison. The first one is the early HQ design (HWP optic axis at $\theta_c = 15^{\circ}$ and QWP $\theta_c = 75^{\circ}$) [17]. In the following discussion, a typical reactive mesogence RM 257 [32] is used in simulating the HQ design, with central wavelength as $\lambda_c = 533$ nm. The second one is an old MTR design (3TR QW-A) in previous work [27], with MTR parameters as: $\phi_0 = 6.4^{\circ}$, $(\phi_1, d_1) = (0^{\circ}, 1.05 \mu m)$, $(\phi_2, d_2) = (43.1^{\circ}, 1.95 \mu m)$, $(\phi_3, d_3) = (83^{\circ}, 0.83 \mu m)$. The validation of previous MTR QWPs is provided in [Supplement 1](#) Fig. S5.

Firstly, the transmittance of the QWPs between crossed polarizers (front polarizer transmission axis $P_1 = 0^{\circ}$ and back polarizer $P_2 = 90^{\circ}$) are investigated. With the unpolarized light Jones vector input as $E_i = (A_s, A_p)^T = (1, 1)^T$, and considering the major reflection loss of the interface between the polarizer and the QWP, the best quarter-wave performance should result in around 46% transmittance. In Fig. 2(a), all four QWPs show relatively high transmittance (>40%) on normal incidence within visible region, proving the stable achromaticity. In some cases the transmittance T exceeds 46%, for example, the T_C in wavelength range (460 nm, 550 nm) and T_A in (420 nm, 520 nm), suggesting that more than half of the total intensity is transmitted through the analyzer. This is due to the fact that the resulted polarization ellipse has its long axis parallel to the analyzer transmission axis. Another important fact is the HQ design shows lowest average transmittance because the optic axis is not continuous for the HWPs and QWPs, thus it has more energy lost compared to the self-aligned MTR structure.

To fully understand the output polarization generated by the MTR QWPs, three other parameters, the ellipticity χ and phase retardation Γ , and the equivalent optic axis Φ is simulated with only polarizer and QWPs. Generally, a perfect QWPs with optic axis $\Phi = 45^{\circ}$ imposes phase retardation $\Gamma = 90^{\circ}$ onto the horizontal linear polarized light, and generates output light with polarized ellipticity $\chi = 45^{\circ}$. The ellipticity χ can be calculated by the output Stokes vector $S' = (S'_0, S'_1, S'_2, S'_3)^T$ in Eq. (5) and the result is shown in Fig. 2(b). For description convenience, the ellipticity, transmission and retardation of HQ, 3TR QW-A, 3TR QW-C, 3TR QW-D is denoted with subscript HQ, A, C, D, respectively. It can be seen that while the maximum of χ_{HQ} at its peak wavelength at green ($\lambda_c = 533$ nm), and falls at blue ($\lambda_c = 457$ nm) and red ($\lambda_c = 636$ nm). The ellipticity χ_A is relatively higher around red and the χ_C is substantially higher in blue, and χ_D has relatively less fluctuation around 45° . The average ellipticity angle $\bar{\chi}$ of the four QWPs can refers to Table 2. It can be seen that $\bar{\chi}_D$ is closest to 45° with wider operational

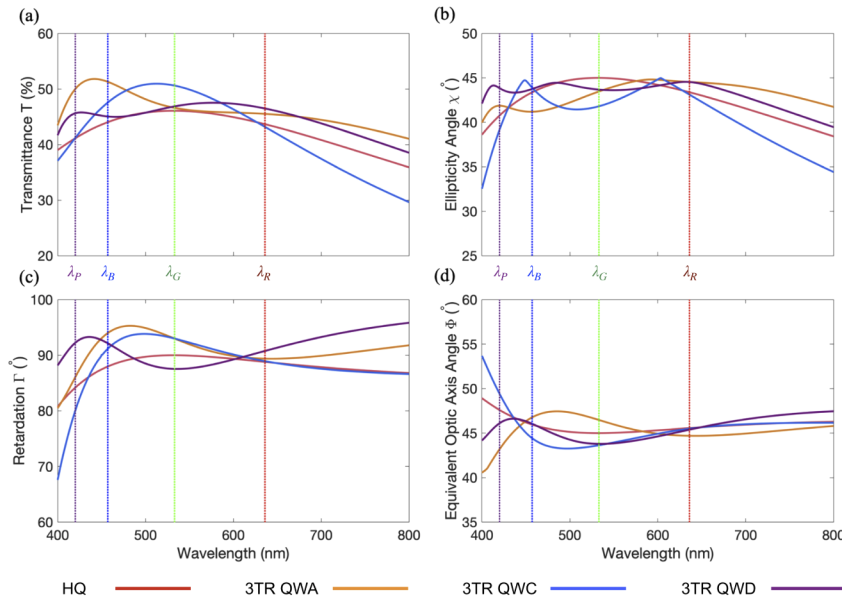


Fig. 2. (a) Simulated transmittance T of four types of QWPs between cross polarizers on normal incidence. (b) Simulated ellipticity angle χ (c) phase retardation Γ and (d) equivalent optic axis angle Φ from the output light of horizontal polarizer and QWPs on normal incidence. The central wavelength is set as : $\lambda_p = 420$ nm , $\lambda_B = 457$ nm, $\lambda_G = 533$ nm, $\lambda_R = 636$ nm.

bandwidth (from 420 nm to 636 nm) , suggesting it's a best achromatic QWP compared to other three in normal incidence.

Table 2. Quarter-Wave Plates On-Axis Performance

QWPs	\bar{T} (%)	ΔT (%)	$\bar{\chi}$ (°)	$\Delta \chi$ (°)	$\bar{\Gamma}$ (°)	$\Delta \Gamma$ (°)	$\bar{\Psi}$ (°)	$\Delta \Psi$ (°)
HQ	43.7	4.9	-43.1	4.2	-87.7	5.8	46.0	2.6
3TR QW-A	48.4	5.8	-42.8	3.3	-87.1	3.4	45.3	3.6
3TR QW-C	45.6	9.4	-42.0	4.7	-86.2	8.9	45.7	5.8
3TR QW-D	46	1.8	-44.1	0.9	-88.1	1.7	45.3	2.3

These findings can also be validated in the phase retardation Γ (Fig. 2(c)), in which the 3TR QW-C has less retardation gap to 90° at blue ($\lambda_c = 457$ nm), while the fluctuation of Γ_D is least within visible wavelength, with smaller retardation deviation $\Delta\Gamma_D$ (Table 2). As mentioned above, the phase retardation of MTR structure can be calculated through the sum of the phase shift of the propagation matrix, or directly from the spherical trigonometry constructed by the input output Stokes vectors on Poincare sphere [18].

Next, we investigate the equivalent optic axis variation of the QWPs on normal incidence. To find the equivalent optic axis, we employ the rotation concept of Poincare sphere. First, we transfer the input/output Jones vector E_i and E' to their corresponding Stokes vector S_i and S' , and put them onto Poincare sphere. Second, we find the geometrical rotational axis (2Φ) on S_1S_2 plane surface that can rotate the S_i to S' [18]. It can be seen that the equivalent optic axis Φ_A reaches 45° at red, and Φ_C reaches 45° at blue and red, while the Φ_D has least fluctuation around 45° (Fig. 2(d)) by smaller $\bar{\Gamma}_D$ (Table 2). These findings agree with the transmittance, ellipticity and retardation result above.

To visualize the process of S_i accumulating the phase retardation Γ and transfer to target output Stokes vector S_t , the Stokes vector trajectory on Poincare sphere is plotted for normal incidence. In Fig. 3(a)-(d), the input Stokes vector setting is set as $S_i = (1, 1, 0, 0)^T$, while the target output is set as $S_t = (1, 0, 0, -1)^T$. It can be seen that all four QWPs have best quarter-wave performance at green, with blue and red fall in the close vicinity of S_t . For violet $\lambda = 420$ nm, all QWPs show relatively large distance from S_t except the 3TR QW-D (Fig. 3(d)) with three chiral layers, shows significantly wide range of operational wavelength from (420 nm, 636 nm), further proving that 3TR QW-D has the best achromaticity among the four.

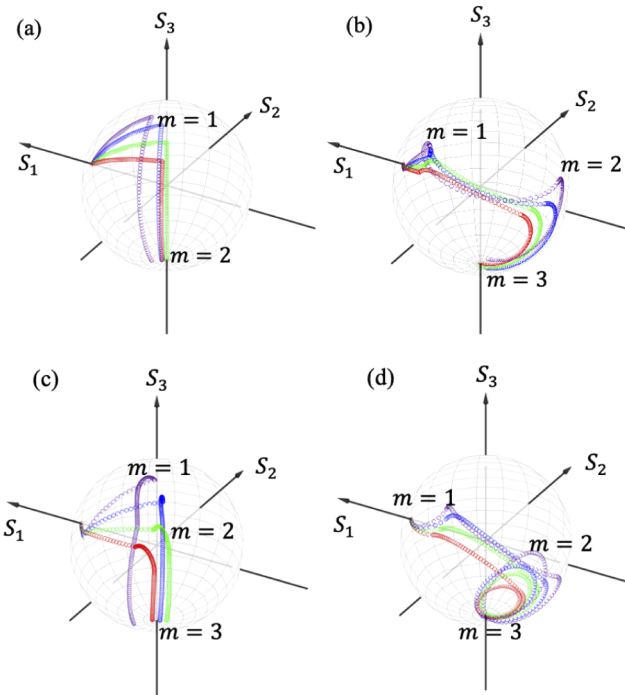


Fig. 3. Stokes vector trajectory on Poincare sphere of incident wavelength $\lambda_P = 420$ nm (purple), $\lambda_B = 457$ nm (blue), $\lambda_G = 533$ nm (green), $\lambda_R = 636$ nm (red) in normal incidence of (a) HQ design; (b) 3TR QW-A; (c) 3TR QW-C; (d) 3TR QW-D.

4.2. Oblique incidence

To have a preliminary check on the wide-angle property of QWPs, we first examine the transmittance of QWPs between cross polarizers with polarizer setting similar as mentioned above (Validation see [Supplement 1](#) Figs. S1 and S2). The transmittance T for four QWPs are plotted for polar angle θ and azimuth angle ϕ on four central wavelength (Fig. 4). Here the polar angle range 45° is chosen based on the requirement of the AR/VR system FOV mentioned before. It can be seen that compared to HQ design, all the MTR QWPs exhibit wider angle for transmittance around center. However as mentioned above, the transmittance can be influenced by several factors, it's not intuitive to compare these three QWPs solely based on the transmittance pattern between cross polarizers.

To fully understand the wide-angle property of QWPs, the polar pattern of ellipticity χ and can be similarly calculated by varying incident angle in different polar and azimuth angle by the output Jones vectors (Fig. 6). It can be seen that all three MTR QWPs have better wide angle performance with RGB range ($\lambda \in (457$ nm, 636 nm)), compared to HQ design. If we choose the

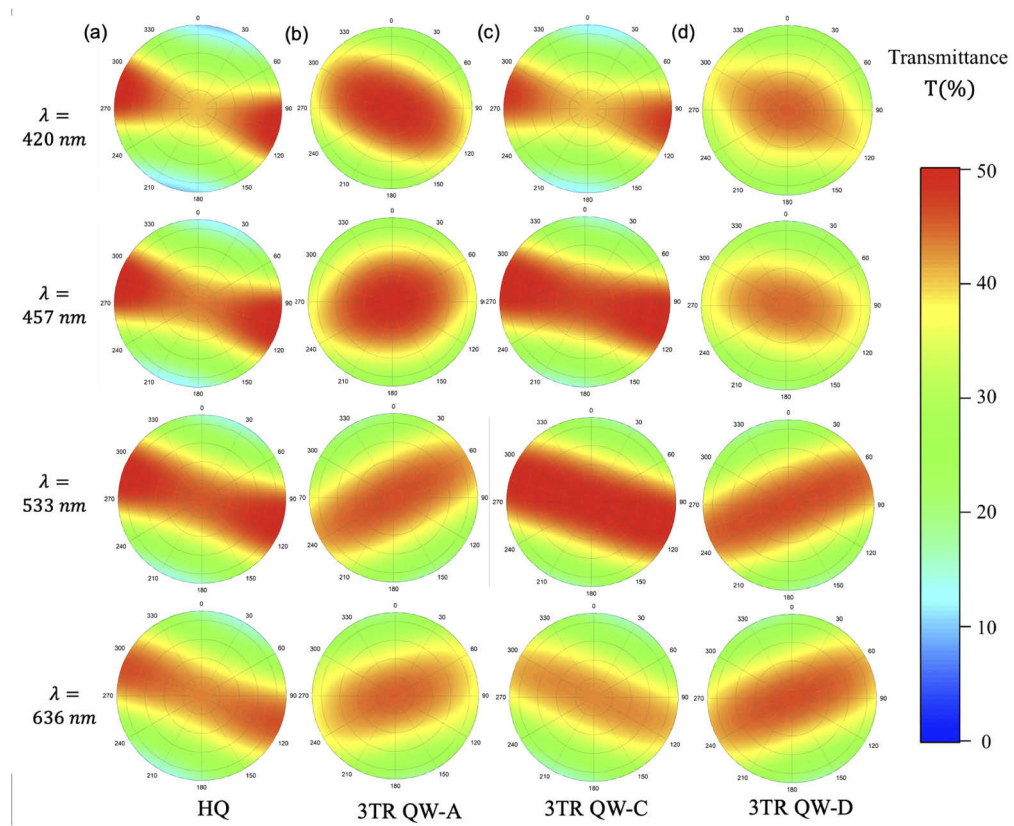


Fig. 4. Transmittance polar pattern of four types QWPs in four central wavelength. Polar angle range is $(0^\circ, 45^\circ)$. Polarizer index $n_p = 1.5$. The front and back polarizer has the transmission axis $p_1 = 0^\circ$ and $p_2 = 90^\circ$ respectively.

central wavelength within this range, almost all MTR QWPs in discussion can have relatively satisfactory wide-angle performance, with average ellipticity of RGB larger than 30° . But if we consider the FWHM of blue LED and include the violet ($\lambda_c = 420 \text{ nm}$), the 3TR QW-D will be the best option.

To evaluate the average ellipticity angle of each QWPs, the off-axis average ellipticity angle and fluctuation of four QWPs listed in Table 3 for polar angle $\theta \in (0^\circ, 30^\circ)$ and Table 4 for $\theta \in (0^\circ, 45^\circ)$. From these two tables, we can conclude that the 3TR QW-D has the highest average ellipticity angle and smallest ellipticity fluctuation among these four. To be specific, within visible visible wavelength the average ellipticity of 3TR QW-D $\bar{\chi}_D = 43.5^\circ$ within $\theta \in (0^\circ, 30^\circ)$, and $\bar{\chi}_D = 42.7$ within $\theta \in (0^\circ, 45^\circ)$. Similar tables of average retardation listed in [Supplement 1](#) Tables S2 and S3 also confirm this result.

Table 3. Quarter-Wave Plates Off-Axis Ellipticity (Unit:°) for $\theta \in (0^\circ, 30^\circ)$

QWPs	$\bar{\chi}(\lambda_P)$	$\Delta\chi(\lambda_P)$	$\bar{\chi}(\lambda_B)$	$\Delta\chi(\lambda_B)$	$\bar{\chi}(\lambda_G)$	$\Delta\chi(\lambda_G)$	$\bar{\chi}(\lambda_R)$	$\Delta\chi(\lambda_R)$
HQ	-40.2	10.1	-42.3	7.9	-43.3	6.4	-42.6	7.4
3TR QW-A	-41.7	5.9	-41.1	6.1	-43.1	4.2	-44.1	3.7
3TR QW-C	-38.9	11	-43	5.7	-41.8	6.6	-43	6.1
3TR QW-D	-43.6	2.9	-43.2	3.3	-43.2	4.1	-44	4.1

Table 4. Quarter-Wave Plates Off-Axis Ellipticity (Unit:°) for $\theta \in (0^\circ, 45^\circ)$

QWPs	$\bar{\chi}(\lambda_P)$	$\Delta\chi(\lambda_P)$	$\bar{\chi}(\lambda_B)$	$\Delta\chi(\lambda_B)$	$\bar{\chi}(\lambda_G)$	$\Delta\chi(\lambda_G)$	$\bar{\chi}(\lambda_R)$	$\Delta\chi(\lambda_R)$
HQ	-38.4	17.7	-40.1	15.8	-41.2	14.4	-41	15.1
3TR QW-A	-40.6	11.4	-40.3	12.9	-42.2	9.9	-43.3	7.5
3TR QW-C	-37.7	18.6	-41.1	12.3	-40.8	10.1	-42	12.3
3TR QW-D	-43.3	7.4	-42.3	8.4	-42.2	10.1	-43	9.6

Second, we investigate the equivalent optic axis variation. It should be noted that the optic axis orientation is a critical parameter when the QWPs is used in reflection leakage system, where QWPs is sandwiched by linear polarizer and mirror. In this circumstance, the linear input light transmits the specific QWPs back and forth. If the optic axis orientation does not bisect the desired slow/fast axis, the reflected light cannot be eliminated and thus leakage occurs. From Fig. 5, it can been seen that HQ has the most severe change of equivalent optic axis and the three MTR QWPs have relatively less variation from ideal optic axis orientation $\Phi = 45^\circ$. Compared to the previous work 3TR QW-A, the 3TR QW-C has much less variation in blue λ_B , but at the expense of gaining variation on the edge in green λ_G . Both of these two design suffered large variation in purple λ_P . For the 3TR QW-D, it has relatively balance performance on green and blue, while keeping low variation on purple. Therefore, we can visualize that the 3TR QW-D can have a better performance in the reflection system. As reference, we also plot the polar pattern of retardation of these four QWPs in [Supplement 1](#) Fig. S6. For the retardation, we find that it matches exactly the pattern of the ellipticity in Fig. 6. This can be understood by the fact that the phase retardation and ellipticity are closely related because the QWPs retardation is the cause of the ellipticity change from linear polarization to circular polarization.

4.3. Reflection luminance leakage

As mentioned before, the orientation of equivalent optic axis is crucial for the reflection system. In this section, we investigate this influence by studying a simple system composed by mirror, QWPs and linear polarizer.

In this section, we will investigate the reflection luminance leakage of these four types of QWPs. The configuration of leakage measurement is depicted in Fig. 7. The QWPs is sandwiched between the horizontal polarizer (Pol 0°) and ideal mirror, with unpolarized broadband light with uniform spectral power distribution (SPD). Under the condition of normal incidence and perfect QWPs, horizontal polarized light E_1 transmits through QWPs and becomes left-hand-circular (LHC) polarized E_2 , which is reflected as right-hand circular (RHC) polarized E_3 and transmits backward through QWPs and produces vertical polarized E_4 . Under such perfect condition, the phase retardation accumulated from this two-fold path is half-wave, therefore no leakage occurs. However, considering the finite achromaticity of actual QWPs, leakage E_5 still occurs when the retardation is not fully quarter-wave at some wavelength even if at normal incidence. For the case of oblique incidence, the birefringence difference due to incident angle causes more severe retardation deviation and thus leakage E_5 is more prominent than that in normal incidence.

To simulate the configuration in Fig. 7, each element can be expressed by the extended Jones matrix itself including the ideal mirror and the QWPs. The propagation of light, either forwards, and backwards, can be simulated using polarization ray tracing matrix [33]. We assume the input unpolarized light as: $E_{in} = [A_s, A_p]^T = [1, 1]^T$. Therefore, the reflection leakage L can be defined as:

$$L = L_5/L_1 \quad (8)$$

where L_1 and L_5 as the lumen of Jones vector E_1 and E_5 in Fig. 7, respectively. To validate the reflection system in Fig. 7, we simulated a HQ design with ideal polarizers and compared it to a

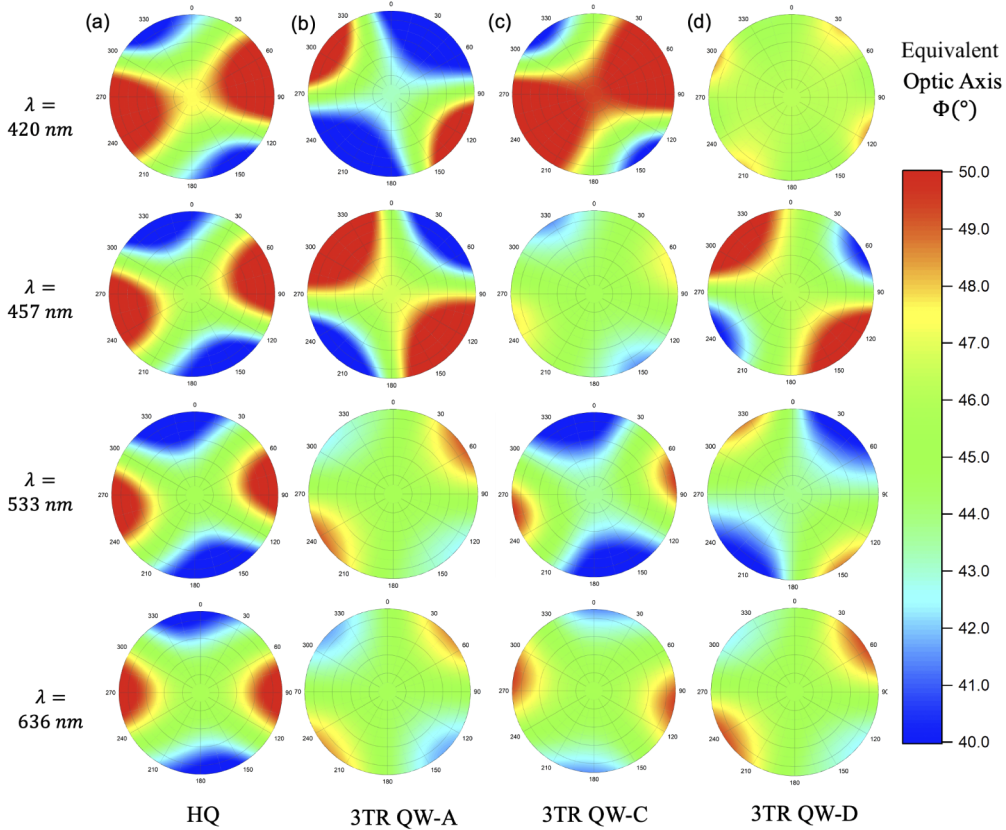


Fig. 5. Equivalent optic axis of four types QWPs in four central wavelength. Polar angle range is $(0^\circ, 45^\circ)$.

published result of commercial software *TechWiz*[26] (See *Supplement 1* Fig. S7). We find that the polar pattern of the HQ design perfectly matches the commercial software result, validating the reflection luminance leakage system and the polarization ray-tracing algorithm is correct.

In order to distinguish the influence of the polarizer off-axis leakage and that of the QWPs, in the following we implement two sets of simulation. First, we simulate a case with perfect polarizer, ignoring Fresnel reflection of the polarizer surface and the polarizer leakage. In this way, any off-axis leakage examined is originated from the QWPs. Second, we simulate a case with real polarizer. The real polarizer setting is just O-type polarizer we mentioned before.

There are several metrics to compare the reflection leakage. Within a certain polar angle range, the maximum leakage $\max(L)$, and the average leakage \bar{L} can be appropriate options. In the ideal polarizer case (Fig. 8) and Table 5, it can be seen that 3TR QW-D has the best off-axis performance in both metrics, with average leakage $\bar{L}_D = 0.18\%$ and maximum leakage $\max(L) = 0.38\%$ in polar angle $\theta \in (0^\circ, 30^\circ)$. The classic HQ design shows better off-axis performance within $\theta \in (0^\circ, 30^\circ)$ compared to 3TR QW-C, but its leakage quickly deteriorates in large polar angle when polar angle range expands to $\theta \in (0^\circ, 45^\circ)$, in which all three MTR QWPs show absolute advantage compared to HQ in both metrics, with 3TR QW-D remained as the lowest leakage QWPs.

In the case of real polarizers, both the QWPs and the polarizers leakages are addressed and the reflection leakage is generally decreased due to the Fresnel reflection loss in the polarizer surface. However, the trend is still similar to the ideal polarizer case. The 3TR QW-D has the

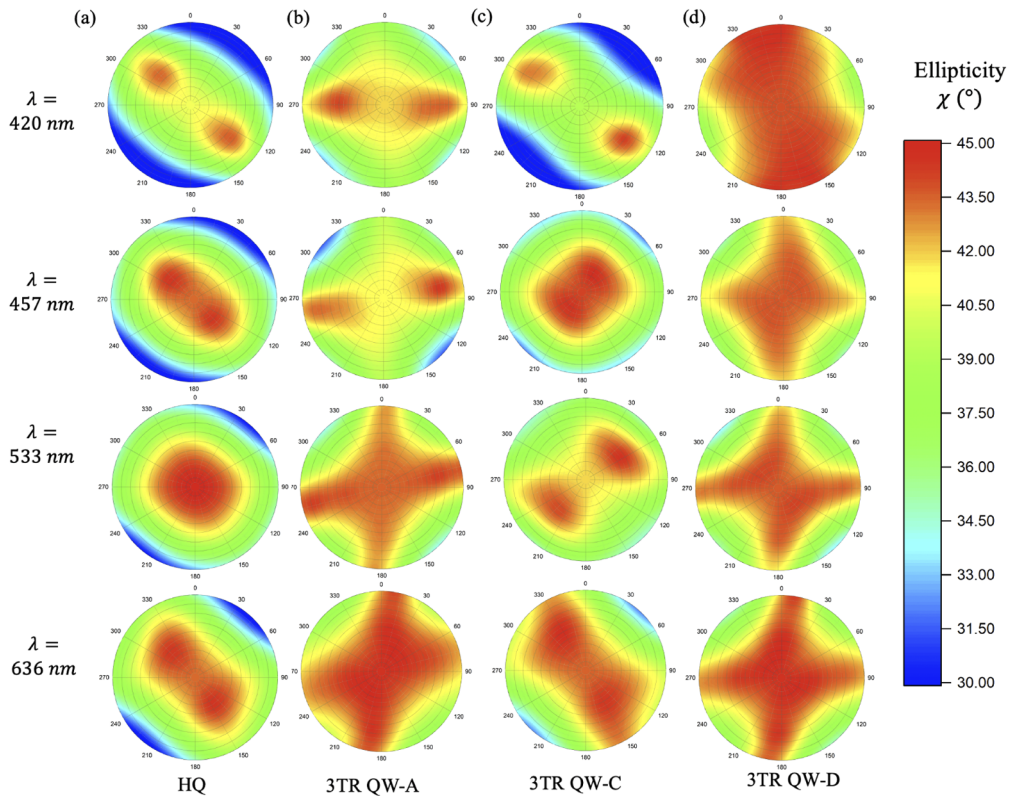


Fig. 6. Ellipticity of four types QWPs in four central wavelength. Polar angle range is $(0^\circ, 45^\circ)$.

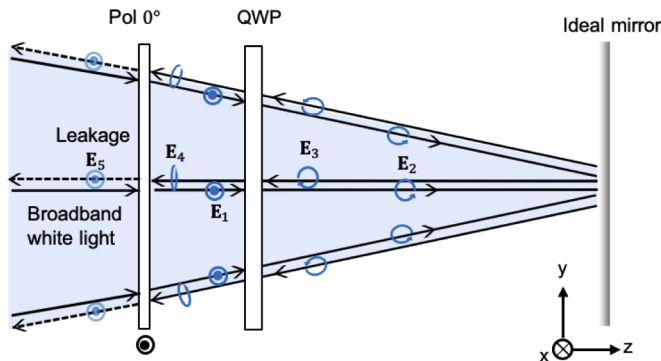


Fig. 7. Configuration of leakage measurement of normal/oblique incidence. The QWPs is sandwiched between the horizontal polarizer (Pol 0°) and ideal mirror, with uniform unpolarized broadband white light as light source. The linear polarized light goes through two-fold optical path within the setup of polarizer-QWPs-mirror, with each stage denoted as Jones vector (E_1 , E_2 , E_3 , E_4 , E_5), and their polarization indicated. The leakage E_5 occurs when the QWPs retardation is not fully quarter-wave.

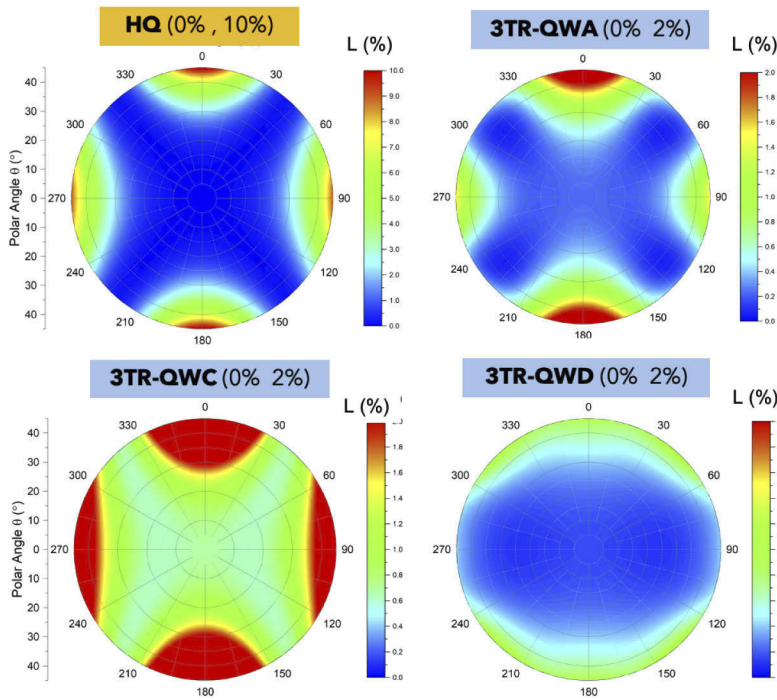


Fig. 8. Iso-luminance pattern of four types of QWPs. Polarizer is simulated as perfect polarizer, with input intensity as 1 and no Fresnel reflection and off-axis leakage. Polar angle range is $(0^\circ, 45^\circ)$.

Table 5. QWPs Leakage with Ideal Polarizer (Unit: %)

QWPs	$\bar{L}(\theta \leq 30^\circ)$	$\max(L)(\theta \leq 30^\circ)$	$\bar{L}(\theta \leq 45^\circ)$	$\max(L)(\theta \leq 45^\circ)$
HQ	0.26	2.01	1.06	9.75
QW-A	0.26	0.83	0.39	2.69
QW-C	0.77	1.96	1.09	5.80
QW-D	0.18	0.38	0.26	0.96

lowest minimum average lumen $L_D = 0.15\%$ (Fig. 9) and maximum leakage $\max(L) = 0.23\%$ in polar angle $\theta \in (0^\circ, 30^\circ)$ (Table 6). In the above analysis, we limit the interest polar angle within $\theta \leq 45^\circ$. However, if we expand the polar angle range up to 90° , it can be seen that 3TR QW-D still has less leakage (maximum leakage 2.8 %) compared to the complicated QWPs composed by positive/negative birefringence and *c*-plate [29] (See Supplement 1 Fig. S8).

Table 6. QWPs Leakage with Real Polarizer (Unit: %)

QWPs	$\bar{L}(\theta \leq 30^\circ)$	$\max(L)(\theta \leq 30^\circ)$	$\bar{L}(\theta \leq 45^\circ)$	$\max(L)(\theta \leq 45^\circ)$
HQ	0.23	1.60	0.69	5.88
3TR QW-A	0.18	0.30	0.20	0.97
3TR QW-C	0.51	0.80	0.58	2.14
3TR QW-D	0.15	0.23	0.17	0.61

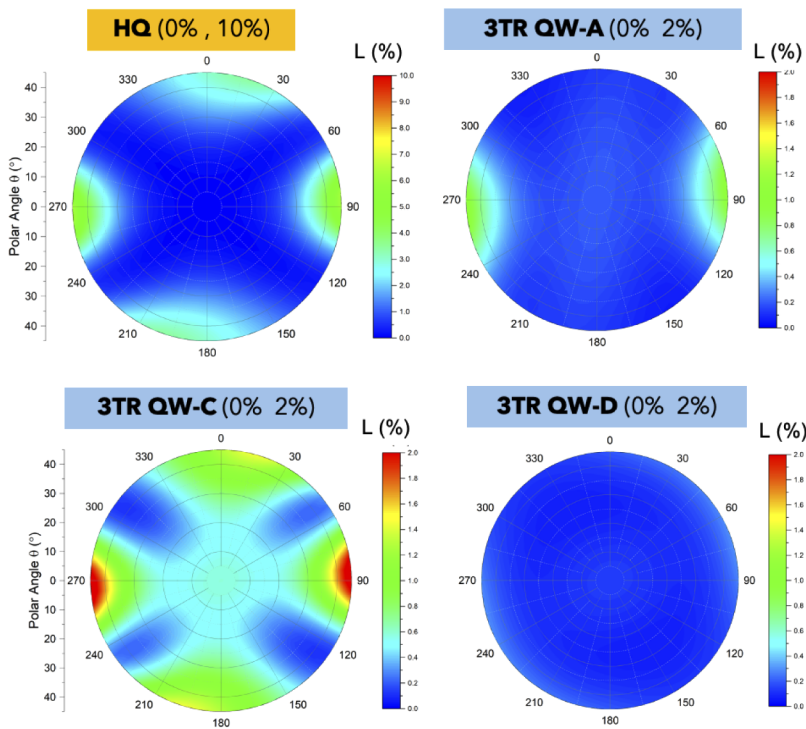


Fig. 9. Iso-luminance pattern of four type of QWPs. Polarizer is simulated as real polarizer (index $n_p = 1.5$), with light source intensity as 1, and Fresnel reflection and off-axis leakage are addressed. Polar angle range is $\theta \in (0^\circ, 45^\circ)$.

5. Conclusion

We theoretically proposed two new designs of multi-twist retarders (MTR) quarter-wave plates (QWPs), 3TR QW-C and 3TR QW-D. The analysis of normal/oblique incidence show that all MTR QWPs can achieve average ellipticity angle up to 40° within polar angle 45° compared to 36° traditional HQ design in primary colors. One type of MTR QWPs (3TR QW-D) has satisfactory wide-angle performance ($AOI \leq 45^\circ$) and super achromaticity from violet to red with average ellipticity 43° within polar angle 30° . This new proposed MTR QWPs is also reported to obtain low average leakage 0.15% and and maximum leakage $\max(L) = 0.23\%$ within polar angle 45° . We believe that the achromaticity and the wide-angle property make this type of monolithic QWPs a promising element in the polarization control of both current and next-generation displays.

Funding. North Carolina State University (2014-2450).

Disclosures. The authors declare no conflicts of interest.

Supplemental document. See [Supplement 1](#) for supporting content.

References

1. M. Ishiguro, K. Ohmuro, Y. Saitoh, Y. Takahashi, J. Watanabe, T. Arai, Y. Ito, and K. Mihayashi, “A novel quarter-wave retardation film for improving viewing angle properties in time-sequential stereoscopic 3d-lcds,” *J. Soc. Inf. Disp.*, **20**(11), 598–603 (2012).
2. P. J. Bos, “Stereoscopic imaging system with passive viewing apparatus,” (1988). US Patent 4, 719, 507.
3. Y. Geng, J. Gollier, B. Wheelwright, F. Peng, Y. Sulai, B. Lewis, N. Chan, W. Sze, T. Lam, A. Fix, D. Lanman, Y. Fu, A. Sohn, B. Bryars, N. Cardenas, Y. Yoon, and S. McEldowney, “Viewing optics for immersive near-eye displays:

- pupil swim/size and weight-stray light," in *Digital Optics for Immersive Displays*, vol. 10676 (International Society for Optics and Photonics, 2018), p. 1067606.
- 4. J. A. LaRussa and A. T. Gill, "The holographic pancake window tm," in *Visual Simulation and Image Realism I*, vol. 162 (International Society for Optics and Photonics, 1978), pp. 120–129.
 - 5. T. L. Wong, Z. Yun, G. Ambur, and J. Etter, "Folded optics with birefringent reflective polarizers," in *Digital Optical Technologies 2017*, vol. 10335 (International Society for Optics and Photonics, 2017), p. 103350E.
 - 6. X. Xiang, J. Kim, and M. J. Escutie, "Bragg polarization gratings for wide angular bandwidth and high efficiency at steep deflection angles," *Sci. Rep.* **8**(1), 7202 (2018).
 - 7. Y.-H. Lee, K. Yin, and S.-T. Wu, "Reflective polarization volume gratings for high efficiency waveguide-coupling augmented reality displays," *Opt. Express* **25**(22), 27008 (2017).
 - 8. S. Moon, C. K. Lee, S. W. Nam, C. Jang, G. Y. Lee, W. Seo, G. Sung, H. S. Lee, and B. Lee, "Augmented reality near-eye display using Pancharatnam-Berry phase lenses," *Sci. Rep.* **9**(1), 6616 (2019).
 - 9. S. Moon, S. W. Nam, Y. Jeong, C. K. Lee, H. S. Lee, and B. Lee, "Compact Augmented Reality Combiner Using Pancharatnam-Berry Phase Lens," *IEEE Photonics Technol. Lett.* **32**(5), 235–238 (2020).
 - 10. L. Li, J. Kim, S. Shi, and M. J. Escutie, "Color-selective geometric phase lens for apochromatic lens system," in *Liquid Crystals XXIV*, vol. 11472 (International Society for Optics and Photonics, 2020), p. 1147219.
 - 11. Z. He, X. Sui, G. Jin, and L. Cao, "Progress in virtual reality and augmented reality based on holographic display," *Appl. Opt.* **58**(5), A74 (2019).
 - 12. N. PrimerovJ. DahdahS. GloorT. von NiederhäusernM. MatuschekA. CastigliaM. MalinvernC. MounirM. RossettiM. DuelkC. Vélez, "A compact red-green-blue superluminescent diode module: A novel light source for ar microdisplays," in *Digital Optical Technologies 2019*, vol. 11062 (International Society for Optics and Photonics, 2019), p. 110620F.
 - 13. V. Tuomas, T. Jani, and P. Pasi, "Waveguide exit pupil expander with improved intensity distribution," (2017). WO Patent WO2017180404.
 - 14. T. Levola, "Diffractive optics for virtual reality displays," *J. Soc. Inf. Disp.* **14**(5), 467 (2006).
 - 15. J. Gollier, B. Wheelwright, and B. D. Silverstein, "Head mounted display with wide field of view and inset display," (2020). US Patent App. 16/287, 785.
 - 16. J. K. T. Tervo, "Large-field-of-view waveguide supporting red, green, and blue in one plate," (2019). US Patent 10, 393, 930.
 - 17. G. Destriau and J. Prouteau, "Réalisation d'un quart d'onde quasi achromatique par juxtaposition de deux lames cristallines de même nature," *J. Phys. Radium* **10**(2), 53–55 (1949).
 - 18. S. Pancharatnam, "Achromatic combinations of birefringent plates," in *Proceedings of the Indian Academy of Sciences-Section A*, vol. 41 (Springer, 1955), pp. 137–144.
 - 19. T. Ishinabe, T. Miyashita, and T. Uchida, "Lp-6: Design of a quarter wave plate with wide viewing angle and wide wavelength range for high quality reflective lcds," in *SID Symposium Digest of Technical Papers*, vol. 32 (Wiley Online Library, 2001), pp. 906–909.
 - 20. Y. Takahashi, Y. Furuki, S. Yoshida, T. Otani, M. Muto, Y. Suga, and Y. Ito, "29.1: A new achromatic quarter-wave film using liquid-crystal materials for anti-reflection of oleds," in *SID Symposium Digest of Technical Papers*, vol. 45 (Wiley Online Library, 2014), pp. 381–384.
 - 21. B. C. Kim, Y. J. Lim, J. H. Song, J. H. Lee, K.-U. Jeong, J. H. Lee, G.-D. Lee, and S. H. Lee, "Wideband antireflective circular polarizer exhibiting a perfect dark state in organic light-emitting-diode display," *Opt. Express* **22**(S7), A1725–A1730 (2014).
 - 22. Q. Hong, T. X. Wu, X. Zhu, R. Lu, and S.-T. Wu, "Designs of wide-view and broadband circular polarizers," *Opt. Express* **13**(20), 8318–8331 (2005).
 - 23. Q. Hong, T. X. Wu, R. Lu, and S.-T. Wu, "Wide-view circular polarizer consisting of a linear polarizer and two biaxial films," *Opt. Express* **13**(26), 10777–10783 (2005).
 - 24. Z. Ge, M. Jiao, R. Lu, T. X. Wu, S.-T. Wu, W.-Y. Li, and C.-K. Wei, "Wide-view and broadband circular polarizers for transreflective liquid crystal displays," *J. Disp. Technol.* **4**(2), 129–138 (2008).
 - 25. Z. Ge, R. Lu, T. X. Wu, S.-T. Wu, C.-L. Lin, N.-C. Hsu, W.-Y. Li, and C.-K. Wei, "Extraordinarily wide-view circular polarizers for liquid crystal displays," *Opt. Express* **16**(5), 3120–3129 (2008).
 - 26. S.-W. Oh, S.-H. Kim, J.-M. Baek, and T.-H. Yoon, "Design of an achromatic wide-view circular polarizer using normal dispersion films," *J. Inf. Disp.* **20**(1), 25–30 (2019).
 - 27. R. K. Komanduri, K. F. Lawler, and M. J. Escutie, "Multi-twist retarders: broadband retardation control using self-aligning reactive liquid crystal layers," *Opt. Express* **21**(1), 404–420 (2013).
 - 28. K. J. Hornburg, R. K. Komanduri, and M. J. Escutie, "Highly chromatic retardation via multi-twist liquid crystal films," *J. Opt. Soc. Am. B* **36**(5), D28–D33 (2019).
 - 29. T.-H. Yoon, G.-D. Lee, and J. C. Kim, "Nontwist quarter-wave liquid-crystal cell for a high-contrast reflective display," *Opt. Lett.* **25**(20), 1547–1549 (2000).
 - 30. A. Uchiyama and T. Yatabe, "P-5: Characteristics and applications of new wide-band retardation films," in *SID Symposium Digest of Technical Papers*, vol. 32 (Wiley Online Library, 2001), pp. 566–569.
 - 31. J. S. Gwag, "Optical fine-tuning for improving the dark level of a reflective liquid crystal display," *Appl. Opt.* **56**(7), 1893–1897 (2017).
 - 32. O. L. Parri, K. Adlem, K. Skjonnemand, and D. Wilkes, "Birefringent layer with negative optical dispersion," (2012). US Patent 8, 119, 026.

33. R. A. Chipman, W. S. T. Lam, and G. Young, *Polarized light and optical systems* (CRC press, 2018).